© 2016. Published by The Company of Biologists Ltd | Development (2016) 143, 4193-4202 doi:10.1242/dev.141192

RESEARCH ARTICLE

Nuclei migrate through constricted spaces using microtubule motors and actin networks in *C. elegans* hypodermal cells

Courtney R. Bone, Yu-Tai Chang, Natalie E. Cain, Shaun P. Murphy and Daniel A. Starr*

ABSTRACT

Cellular migrations through constricted spaces are a crucial aspect of many developmental and disease processes including hematopoiesis, inflammation and metastasis. A limiting factor in these events is nuclear deformation. Here, we establish an *in vivo* model in which nuclei can be visualized while moving through constrictions and use it to elucidate mechanisms for nuclear migration. *C. elegans* hypodermal P-cell larval nuclei traverse a narrow space that is about 5% their width. This constriction is blocked by fibrous organelles, structures that pass through P cells to connect the muscles to cuticle. Fibrous organelles are removed just prior to nuclear migration, when nuclei and lamins undergo extreme morphological changes to squeeze through the space. Both actin and microtubule networks are organized to mediate nuclear migration. The LINC complex, consisting of the SUN protein UNC-84 and the KASH protein UNC-83, recruits dynein and kinesin-1 to the nuclear surface. Both motors function in P-cell nuclear migration, but dynein, functioning through UNC-83, plays a more central role as nuclei migrate towards minus ends of polarized microtubule networks. Thus, the nucleoskeleton and cytoskeleton are coordinated to move nuclei through constricted spaces.

KEY WORDS: *C. elegans*, KASH, SUN, Dynein, Nuclear migration

INTRODUCTION

Many cellular migration events, including some in development and metastasis, involve traversing through constricted spaces. For example, hematopoietic cells migrate through small openings in a basement membrane to exit the bone marrow (Junt et al., 2007; Shin et al., 2013). When cells migrate through narrow spaces, the rate of migration is limited by the ability to squeeze the nucleus through the constricted space (Fu et al., 2012; Wolf et al., 2013). The deformability of the nucleus is determined by lamin composition (Swift et al., 2013). When levels of LaminA are elevated, cells migrate more slowly through constrictions, whereas LaminA knockdown cells are able to traverse constrictions faster than wild type (Davidson et al., 2014; Rowat et al., 2013). The nucleus in dendritic cells is aided in deformation by Arp2/3 nucleated actin filaments within the constriction (Thiam et al., 2016). Nuclei in cells migrating through fabricated chambers or collagen matrices tend to rupture from mechanical strain, and are repaired by ESCRT III (Denais et al., 2016; Raab et al., 2016). Although these findings have allowed better understanding of cellular migration through constricted spaces *in vitro*, how nuclei migrate through constrictions *in vivo* is poorly understood. Here, we established *Caenorhabditis elegans* P-cell nuclear migration as a model for nuclear migration through constricted spaces. We found that three molecular components – lamins, microtubule motors and actin networks – were required for this migration.

During the first *C. elegans* larval stage (L1), a series of cellular rearrangements reorganize the hypodermal layer on the animal's ventral surface. At hatching, the ventral surface is covered by 12 P cells (Sulston and Horvitz, 1977). By late L1, P cells retract into the ventral cord and the hyp7 syncytium covers the ventral surface (Altun and Hall, 2009a; Sulston and Horvitz, 1977). During this event, P-cell nuclei migrate from a lateral to a ventral position through a constricted space – approximately 200 nm, or 5% of the pre-migration diameter of the nucleus – between body wall muscles and the cuticle (Cox and Hardin, 2004; Francis and Waterston, 1991). It is unknown whether nuclei flatten to squeeze through the constriction or the constriction swells to allow migration. After nuclear migration, P cells divide and give rise to the vulva, hypodermal cells and motor neurons. Failure of P-cell nuclear migration results in P-cell death and in turn, Egl (egg laying deficient) and Unc (uncoordinated) animals due to the lack of vulval cells and motor neurons, respectively (Horvitz and Sulston, 1980; Sulston and Horvitz, 1981).

Two genes, *unc-83* and *unc-84*, play roles in both embryonic hyp7 precursor and larval P-cell nuclear migration events (Malone et al., 1999; Starr et al., 2001; Sulston and Horvitz, 1981). UNC-83 and UNC-84 are nuclear envelope proteins that interact in the perinuclear space to bridge the nuclear envelope (reviewed by Starr and Fridolfsson, 2010). UNC-83 is an outer nuclear membrane transmembrane protein with a conserved KASH (Klarsicht ANC-1 Syne Homology) domain at its C terminus in the perinuclear space (Starr et al., 2001). UNC-84 is an integral inner nuclear membrane protein with a conserved SUN (Sad1 UNC-84) domain in the perinuclear space (Malone et al., 1999). UNC-84 recruits and interacts with UNC-83 to form a bridge, termed the LINC (linker of nucleoskeleton and cytoskeleton) complex, which spans the nuclear envelope (McGee et al., 2006). This bridge functions to connect nuclei to the cytoskeleton. More specifically, UNC-84 interacts with the single *C. elegans* lamin, LMN-1, in the nucleoskeleton (Bone et al., 2014; Lee et al., 2002) whereas UNC-83 recruits two microtubule motors, cytoplasmic dynein and kinesin-1, to the nuclear envelope to mediate nuclear migration in *C. elegans* embryonic hyp7 precursor cells (Fridolfsson et al., 2010; Fridolfsson and Starr, 2010; Meyerzon et al., 2009).

LINC complexes are conserved throughout eukaryotes and mediate a variety of nuclear migration events from plant pollen-tube migration to mammalian muscle development. However, many LINC-independent mechanisms exist to move nuclei, such as in *Drosophila* oocytes where microtubules push the nucleus from behind (Zhao et al., 2012) and in the mouse neocortex where dynein is recruited to nuclear pore components for apical migration (Bolhy et al., 2011; Splinter et al., 2010).

Department of Molecular and Cellular Biology, University of California, Davis, CA 95616, USA.

*Author for correspondence (dastarr@ucdavis.edu)

D.A.S., 0000-0001-7339-6606

Received 15 June 2016; Accepted 20 September 2016

Development (2016) 143, 4193-4202 doi:10.1242/dev.141192

Although the LINC complex is essential for nuclear migration in *C. elegans* embryonic hyp7 precursors, loss of the LINC complex does not abolish P-cell nuclear migration. Null mutations in *unc-83* or *unc-84* cause a temperature-sensitive nuclear migration defect; less than 40% of P-cell nuclei migrate to the ventral cord at 25°C, but at 15°C at least 90% of nuclei migrate (Malone et al., 1999; Starr et al., 2001). This led to the hypothesis that a parallel pathway was sufficient for P-cell nuclear migration at 15°C in the absence of SUN and KASH bridges. To test this, a mutant screen was conducted in *unc-84* null animals to identify additional players in P-cell nuclear migration, which led to the identification of the actin regulator TOCA-1 (Chang et al., 2013).

Based on our results, we propose that three distinct molecular components ensure P-cell nuclear migration through the constricted region between body wall muscle and the cuticle: nuclear reorganization, the LINC complex with microtubule motors, and actin networks. We hypothesized that nuclear lamins must be reorganized for the nucleus to squeeze into the constricted space as it migrates. Furthermore, we hypothesized that an actin-based pathway functions to assist P-cell nuclear migration. Finally, we hypothesized that microtubule motors, primarily kinesin-1, through the LINC complex provide the force to move nuclei. We used genetics and live imaging to identify molecular components required for P-cell nuclear migration through a constricted space. Nuclei were observed squeezing through the narrow region. In addition, we describe the structure of actin filaments during P-cell nuclear migration. Finally, and in contrast to hyp7 nuclear migration, we found that cytoplasmic dynein was the primary motor for moving P-cell nuclei towards the minus ends of polarized microtubules. Our data establish P-cell nuclear migration as an *in vivo* system to study migration through constricted spaces, which we used to study the roles of three different filaments – lamin, microtubules and actin.

RESULTS

P-cell morphology during larval development

We sought to further characterize P-cell morphological changes during L1 development. Three cell types – P-cells, the hyp7 syncytium, and the seam cells that act as stem cells (Fig. 1, green, tan and blue, respectively) – are involved in this rearrangement of the ventral hypodermis. To characterize P-cell morphology changes, we imaged cell-cell junctions using the adherens junction marker AJM-1 and labeled P cell nuclei with an NLS: tdTomato marker driven by the P-cell-specific promoter for *hlh-3*

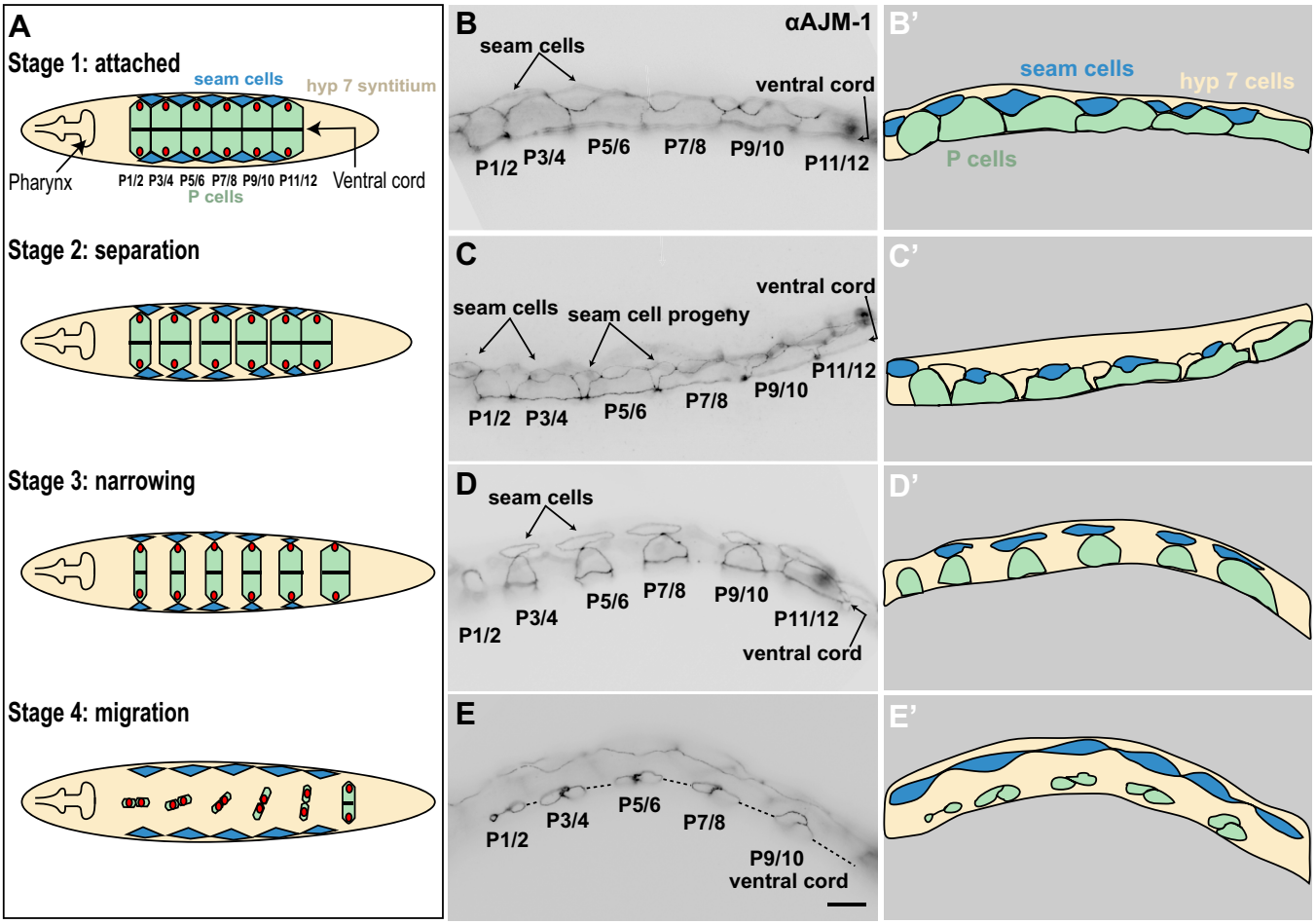

Fig. 1. Stages of P-cell morphology throughout early L1 development. Four stages of P-cell morphological changes are shown. (A) Three cell types are depicted in ventral view: P cells (green), the hyp7 syncytium (tan) and seam cells (blue). Stage 1, attached: 12 P cells organized in six pairs with their nuclei (red) on the lateral side. P cells are attached to their anterior/posterior neighbors to cover the ventral surface completely. Stage 2, separation: P cells separate from their neighbors and hyp7 cells fill the openings. Stage 3, narrowing: P cell pairs narrow and hyp7 cells expand to fill the resulting spaces. Stage 4, migration: Nuclei migrate from lateral to ventral. Anterior pairs of P cells migrate first. By the end of migration the P-cell cytoplasm retracts to the ventral cord. (B-E) Lateral views of the four stages of fixed larvae stained with an anti-AJM-1 antibody to mark adherens junctions. (B′-E′) The same images pseudocolored to identify cell types. Scale bar: 10 µm.

Development (2016) 143, 4193-4202 doi:10.1242/dev.141192

(Chang et al., 2013; Doonan et al., 2008; Koppen et al., 2001) (Fig. 1).

Four distinct phases of P-cell shape changes were observed: attached, separation, narrowing and migration (Fig. 1). At hatching, P cells were attached to each other in two rows of six across the ventral cord, with nuclei positioned at the lateral ends (Fig. 1A stage 1; Fig. 1B,B′). Shortly after hatching, P cells began to separate from their anterior and posterior neighbors (Fig. 1A stage 2; Fig. 1C,C′). As the six pairs of P cells moved apart, they were interpolated by the expanding hyp7. This process was initiated at the anterior of the animal and moved posteriorly. In the narrowing stage of P-cell development, the ventral hyp7 continued to expand between P cells, while the P cells greatly narrowed along the anterior-posterior axis (Fig. 1A stage 3; Fig. 1D,D′). Throughout the separation and narrowing stages, P-cell nuclei remained at the lateral ends of the cells and P cells continued to stretch from the ventral cord to the lateral seam cells. Nuclear migration occurred in the final phase of P-cell rearrangement (Fig. 1A stage 4; Fig. 1E,E′). P-cell nuclei migrated from their lateral position to the ventral cord. The anterior-most P1 and P2 pair of P-cell nuclei migrated first, followed progressively by the posterior pairs of P cells. The entire process occurred over 2 h, 11-13 h after hatching at 20°C. P cells have a unique shape in cross-section with one bulbous region on the lateral side next to seam cells and a second in the ventral cord (Altun and Hall, 2009b) (Fig. 2A). The cytoplasmic region that connects these two ends is only about 200 nm thick (Cox and Hardin, 2004; Francis and Waterston, 1991). During migration, P-cell nuclei 3-4 µm in diameter must move through this constricted space to get to the ventral cord. After P-cell nuclear migration, the cytoplasm retracts to the ventral cord. This results in 12 P cells entirely in the ventral cord.

Fibrous organelles are disassembled in P cells during the time of P-cell nuclear migration

The P-cell nuclear migration path is obstructed by fibrous organelles, hemidesmosome-like structures in hypodermal cells that serve as part of a mechanical link to connect the cuticle to body wall muscles (Fig. 2A,B) (Altun and Hall, 2009b; Francis and Waterston, 1991). Embryos with defects in fibrous organelles fail to elongate and arrest at the two-fold stage of embryogenesis (Bosher et al., 2003; Hresko et al., 1994). We therefore hypothesized that fibrous organelles are removed prior to P-cell nuclear migration. We followed fibrous organelles using IFB-1::GFP (Woo et al., 2004). IFB-1::GFP forms short lines consisting of the ends of many fibrous organelles (Fig. 2). Parallel lines of fibrous organelles were observed throughout the ventral side of larvae prior to migration (Fig. 2C,D). However, at the time of nuclear migration IFB-1::GFP was no longer visible in P cells (Fig. 2E, P5/6), nor was it visible in the hyp7 immediately after P-cell migration (Fig. 2E, P3/4). Following nuclear migration and P-cell cytoplasmic retraction, fibrous organelles were re-established in the newly formed ventral hyp7 syncytium (see around P1/2 in Fig. 2E). These data show that fibrous organelles are removed in P cells prior to nuclear migration and rebuilt in the hyp7 after migration completes.

P-cell nuclei undergo dramatic morphology changes to squeeze through constricted spaces

There are two models for how P-cell nuclei migrate between muscles and the cuticle to reach the ventral cord. First, the nucleus could undergo shape changes to flatten out and squeeze through the constriction. Alternatively, once the fibrous organelles are removed, the space between muscle and cuticle could expand to allow the

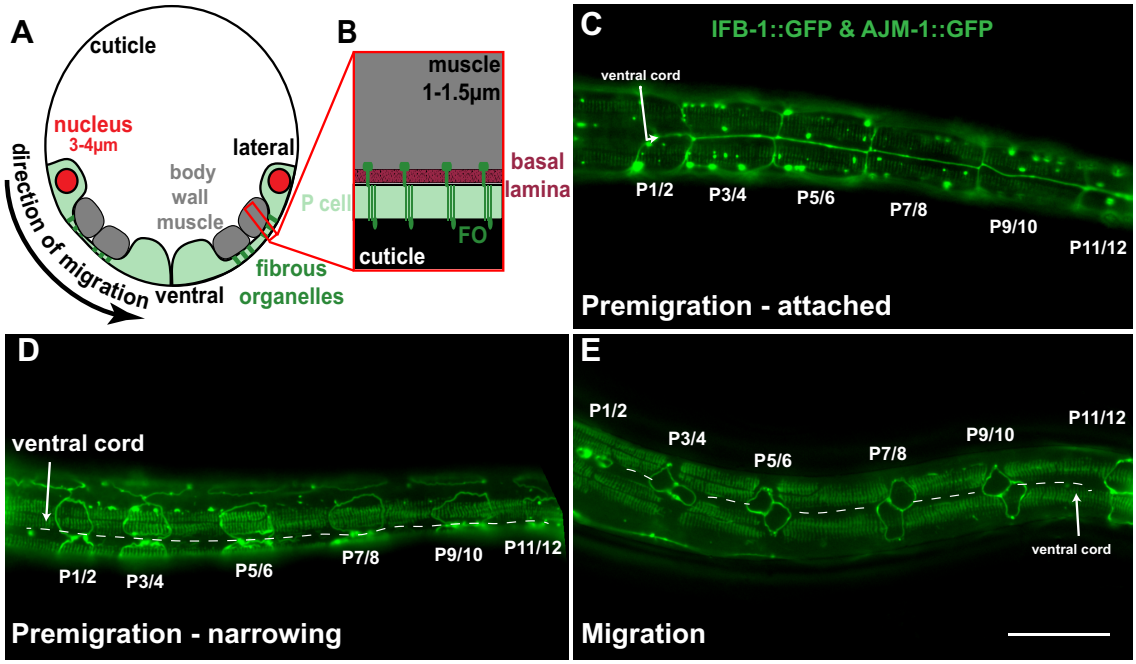

Fig. 2. Fibrous organelles are disassembled in P cells at the time of nuclear migration. (A) A cross-section depicting the shape of P cells. The P cell (green) is constricted between the cuticle (black) and body wall muscles (gray), and the nuclei (red) are on the lateral sides. (B) The cuticle is connected to the body wall muscle through P cells and the basal lamina (maroon) by fibrous organelles (FO, green). (C-E) Animals were visualized expressing both AJM-1::GFP and IFB-1::GFP to visualize fibrous organelles. Large aggregates, particularly in C, are an artifact of AJM-1::GFP overexpression. (C) Stage 1, attached. Fibrous organelles are seen 'end on', but line up close to one another and appear in lines. (D) Stage 3, narrowing. Fibrous organelles in P cells (outlined by AJM-1::GFP) and hyp7 between P cells. (E) Stage 4, nuclear migration. Fibrous organelles are absent in P cells during migration (P3/4) and are in the process of disassembling just prior to migration (P7/8). Fibrous organelles are reorganized in the hyp7 syncytium following P-cell cytoplasm retraction to the ventral cord (visible at P1/2). Dashed line represents the ventral cord. Scale bar: 20 µm.

Development (2016) 143, 4193-4202 doi:10.1242/dev.141192

nucleus to migrate between them. To distinguish between these models, transgenic *C. elegans* lines expressing live P-cell markers were generated.

As P-cell nuclei migrate, the nucleus extends and flattens into the constricted space. During migration, nuclear volumes were visualized on both the lateral and ventral sides of the constriction, where the NLS::tdTomato signal was much fainter (Fig. 3B,C, NLS::tdTomato insets). The entire shape of a migrating nucleus was more clearly observed in a *z*-stack (Movie 1), in which it appeared to be divided between ventral and lateral compartments connected by a thin sheet of nucleoplasm (final frames of Movie 1). These images suggested that the nucleus was flattened between muscles and the cuticle (Fig. 3B,C, insets). As the nucleus migrated, the NLS::tdTomato signal volume and intensity increased on the ventral side as it decreased on the lateral side. The process of one nucleus moving through the constriction took over 25 min (Fig. 3E; Movie 2).

Lamin levels and composition are known to affect the ability of nuclei to migrate through constrictions in mammalian tissue culture (Davidson et al., 2014; Rowat et al., 2013). We therefore examined changes in lamins during migration by imaging lamin tagged with GFP at the endogenous *lmn-1* locus using CRISPR/Cas9-mediated genome editing (Arribere et al., 2014; Dickinson et al., 2013; Paix et al., 2015). *C. elegans* have a single lamin gene, *lmn-1*, that is broadly expressed and is essential for early embryonic divisions (Liu et al., 2000). We first determined the extent to which N- or C-terminally tagged lamins were functional. Both GFP fusion proteins localized to the periphery of nearly all nuclei in a pattern similar to anti-LMN-1 antibodies (Fig. S1A,B) (Liu et al., 2000). However, LMN-1::GFP was significantly fainter than GFP::LMN-1. *lmn-1::gfp* homozygous animals laid few embryos, which were non-viable. By comparison, *gfp::lmn-1* animals laid about half the normal number of embryos, and more than 60% of these embryos were viable (Fig. S1C,D). We concluded that GFP::LMN-1 is partially functional and we therefore used it to follow the nucleoskeleton during P-cell nuclear migration.

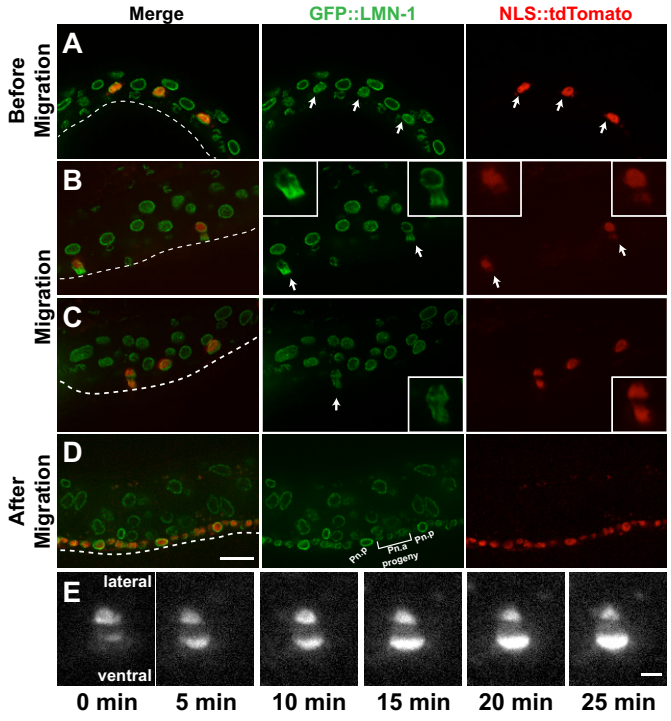

Fig. 3. P-cell nuclei squeeze through constricted spaces. Images of larvae with NLS::tdTomato in P-cell lineages (red, or white in E) and endogenously expressed GFP::LMN-1 (green). All images are lateral views of L1 larvae with ventral (dashed line) down and anterior left. (A) A larva prior to nuclear migration with GFP::LMN-1 surrounding all visible nuclei. Arrows mark P-cell nuclei. (B,C) Larvae at the time of P-cell nuclear migration. P-cell nuclei that are undergoing migration are marked by arrows. Insets show enlarged images of P-cell nuclei during migration. (D) A larva after P-cell migration. (E) A single migrating P-cell nucleus shown over a 25 min period. Images are 5 min apart. Scale bars: 10 µm (A-D); 5 µm (E).

GFP::LMN-1 localized around the nuclear volume of P cells prior to and during nuclear migration (Fig. 3A-C). During nuclear migration, GFP::LMN-1 was visible around both the lateral and ventral volumes of the nucleus and in the constricted space. To determine whether lamin amounts were enriched in the direction of migration, we quantified the ratio of GFP::LMN-1 intensity in the constriction to the intensity in the lateral volume of migrating P-cell nuclei. In 6 of 11 nuclei, the ratio was between 0.8 and 1.3 (mean=0.93), suggesting equal LMN-1 in the constriction versus the lateral surface. However, in 5 of 11 migrating P-cell nuclei, the ratio was between 1.3 and 2.0 (mean=1.63). This could represent biased localization of LMN-1 to the constriction. However, because of limits of resolution in the *z*-plane, the increase in LMN-1 intensity in the constriction is probably due to measuring GFP::LMN-1 on both the inner and outer surfaces of the nucleus, which would push the ratio closer to two. Thus, the intensity of GFP::LMN-1 observed in the constriction was not significantly enriched compared with the peripheral volumes. NLS::tdTomato and GFP::LMN-1 remained visible in P-cell progeny following nuclear migration in the ventral cord (Fig. 3D).

Actin cables extend throughout P cells

Previously, the actin regulator TOCA-1 and actin nucleators in the WAVE/SCAR and Arp2/3 complexes were shown to be involved in P-cell nuclear migration (Chang et al., 2013; Xiong et al., 2011). We therefore characterized actin networks prior to and during nuclear migration, using Lifeact::mKate2, which binds filamentous actin (Riedl et al., 2008) expressed under control of the *hlh-3* promoter. During the attached and early separation stages of P-cell development, actin filaments were enriched at the cellular periphery (Fig. 4A,B, arrows). Some P cells contained thick, apparently continuous cables that extended through the constriction (Fig. 4A; Movies 3, 5, 7). Other P cells had thinner actin filaments that appeared to be less continuous (Fig. 4B; Movies 4, 6). By the time of nuclear migration, all P cells observed contained thick actin cables (Fig. 4F; Movie 8). In addition to cables and filaments, some cells contained an actin ring on the lateral side, close to the nucleus (Fig. 4C,Db, arrowheads). To visualize actin structures present in a single P cell better, six images from a *z*-stack in the separation stage are depicted (Fig. 4Da-f; Movie 6). Actin cables and peripheral enrichment was also visible in the later narrowing stage of P-cell development (Fig. 4E). During nuclear migration, actin cables continued to extend throughout the cell through the constriction and actin rings were visible on the lateral side (Fig. 4F). These data showed that actin structures were present throughout P-cell larval development, consistent with a role for actin in moving P-cell nuclei.

Microtubules are polarized at the time of P-cell nuclear migration

We utilized live imaging of β-tubulin in P cells to determine the contribution of microtubule-based mechanisms to nuclear migration. Microtubules were oriented parallel to the axis of migration as nuclei moved through the constricted space

Development (2016) 143, 4193-4202 doi:10.1242/dev.141192

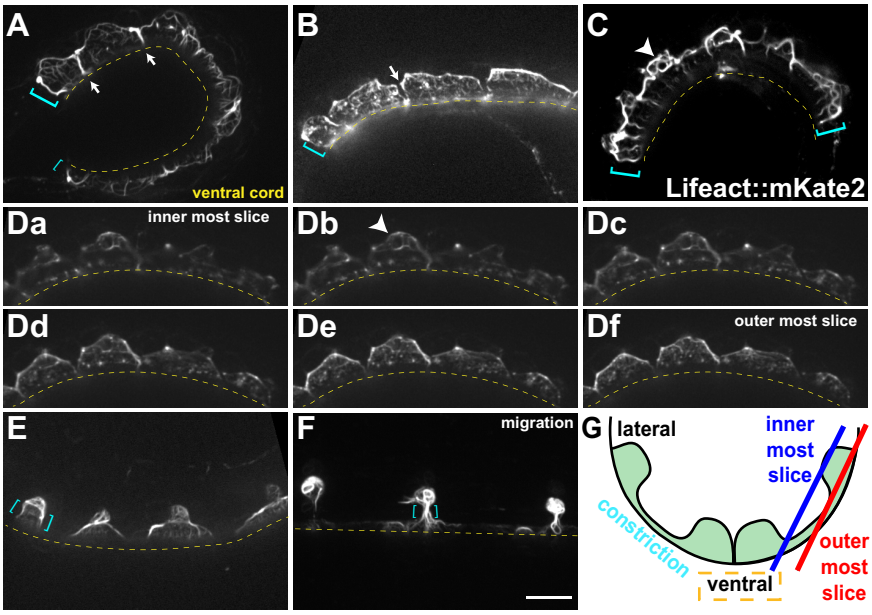

Fig. 4. Actin networks in larval P cells. (A-F) Lifeact::mKate2 expressed in P cells is shown. Lateral views with ventral (dashed line) down and anterior left. Pre-migration stage larval P cells have either thick actin cables (A,C) or thin actin filaments (B,D). Actin is enriched at the cell periphery and cell-cell boundaries (arrows in A,B). Actin rings are seen in some larvae (arrowheads C, Db). (Da-f) A single premigration larva is shown in six images from a *z*-stack (200 nm steps) starting with an interior slice showing the ventral cord followed by images moving up and out to the lateral side. (E) Actin cables and peripheral enrichment in narrowing cells. (F) Actin cables visualized through the constriction (cyan brackets) in migration stage P cells. (G) Schematic depicting a P cell (green) cross-section labeled with the ventral side (yellow dashed line in images), lateral side, and the constriction (cyan brackets in images). Inner and outer boundaries of the *z*-stack shown in D are marked.

(Fig. 5A,B). In embryonic hyp7 precursors, kinesin-1 provides the major force to pull nuclei forward towards the plus ends of microtubules, whereas dynein serves a minor role in allowing nuclei to move backwards and bypass roadblocks (Fridolfsson et al., 2010; Fridolfsson and Starr, 2010; Meyerzon et al., 2009). By contrast, dynein light chain DYRB-1 functions during polarization of intestinal primordial cells, suggesting that dynein plays the major role in other directed nuclear migrations (Feldman and Priess, 2012).

We determined the direction of microtubule growth in the constricted space by following the EB1 homolog EBP-1::GFP in P cells. In Fig. 5C,D, EBP-1::GFP is shown at two different time points (Movies 9, 10). The first time point is pseudocolored magenta and the second, 5 s later, is pseudocolored cyan. We found that prior to nuclear migration, 57.6% of EBP-1::GFP comets grew towards P-cell nuclei from the lateral end, 34.6% grew ventrally in the direction of migration, and 7.7% grew perpendicular to the direction of migration (Fig. 5E). During migration, more EBP-1::GFP comets (84.0%) grew laterally towards P-cell nuclei, only 10.4% of comets grew in the direction of migration, and 5.7% grew perpendicular to the direction of migration (Fig. 5E). Thus, microtubules changed from random orientation in early P-cell development, to growth towards nuclei at migration ($P<0.0001$ by χ^2 contingency test), suggesting that nuclei migrate towards microtubule minus ends.

Microtubule motors function in P-cell nuclear migration

We used RNAi and mutant alleles to test the hypothesis that cytoplasmic dynein is the major force generator to move P-cell nuclei. We scored a failed nuclear migration when a P-cell nucleus (using NLS::tdTomato, as in Fig. 3) remained lateral after the division of P-cell nuclei in the ventral cord, indicating the end of P-cell nuclear migration. We also counted the number of missing GABA neurons marked by UNC-47::GFP (Fig. 6) (Chang et al., 2013; McIntire et al., 1997). In young adulthood, *C. elegans* normally have 19 GABA neurons, 12 of which are derived from P cells, in the ventral cord. These assays were performed at 25°C, the restrictive temperature for *unc-83* and *unc-84* null animals.

Because cytoplasmic dynein is an essential motor, we first performed knockdown of two dynein adaptors, NUD-2 (NDE1 and NDEL1 homolog) and BICD-1 (Bicaudal D homolog) previously shown to function in parallel to recruit dynein to the nuclear envelope (Fridolfsson et al., 2010). We observed an average of 1.8±0.47 [mean±95% confidence interval (CI)] failed migrations in *nud-2(ok949);bicd-1(RNAi)* animals [$P<0.0001$ compared with *nud-2(ok949)* in an unpaired *t*-test; Fig. 6E] and there was a loss of 0.7±0.14 GABA neurons [$P<0.0001$ compared with *nud-2(ok949)* in an unpaired *t*-test; Fig. 6F]. To test more directly the role of dynein, we analyzed animals carrying *dhc-1(js319)*, a dynein heavy chain hypomorphic allele, which probably demonstrates an under-representation of the effects of completely missing dynein. We counted an average of 2.7±0.30 missing GABA neurons in *dhc-1 (js319)* animals [$P<0.0001$ compared with L4440 (empty vector) in an unpaired *t*-test; Fig. 6F]. Thus, dynein plays a significant role in moving P-cell nuclei.

The nuclear migration phenotypes we observed in dynein knockdown animals were less penetrant than in *unc-83* mutants. We therefore investigated the role of kinesin-1 in P-cell nuclear migration by knocking down genes encoding either the kinesin-1 light chain (KLC-2) or heavy chain (UNC-116). We could not use null alleles of *klc-2* or *unc-116*, owing to high levels of embryonic lethality (Meyerzon et al., 2009; Sakamoto et al., 2005). Instead, we used RNAi to partially knockdown *klc-2* and *unc-116*. RNAi efficiency was assayed in these experiments by scoring nuclear migration defects in the dorsal hyp7. In wild-type and mutant backgrounds (see below), both *klc-2(RNAi)* and *unc-116(RNAi)* led to strong dorsal hyp7 nuclear migration defects; an average of 8.6 to 10.4 (with 95% CI<1.1) hyp7 nuclei were observed in the dorsal cord (n=18-121). These values were similar to those previously reported in strong loss-of-function alleles of *klc-2* (Meyerzon et al., 2009). *klc-2(RNAi)* or *unc-116(RNAi)* resulted in 0.7±0.44 and 0.3±0.22 failed nuclear migrations per animal, respectively (Fig. 6E). Furthermore, kinesin-1 knockdown animals were missing only 0.25±0.24 and 0.24±0.20 GABA neurons in *unc-116(RNAi)* or *klc-2(RNAi)* animals, respectively (Fig. 6F). Thus, kinesin-1 appears to play a less important role in P-cell nuclear migration than dynein.

In *dhc-1(js319)* mutant animals, kinesin-1 RNAi significantly enhanced the P-cell nuclear migration defect. *dhc-1(js319); klc-2(RNAi)* animals were missing 5.0±0.76 GABA neurons and

Development (2016) 143, 4193-4202 doi:10.1242/dev.141192

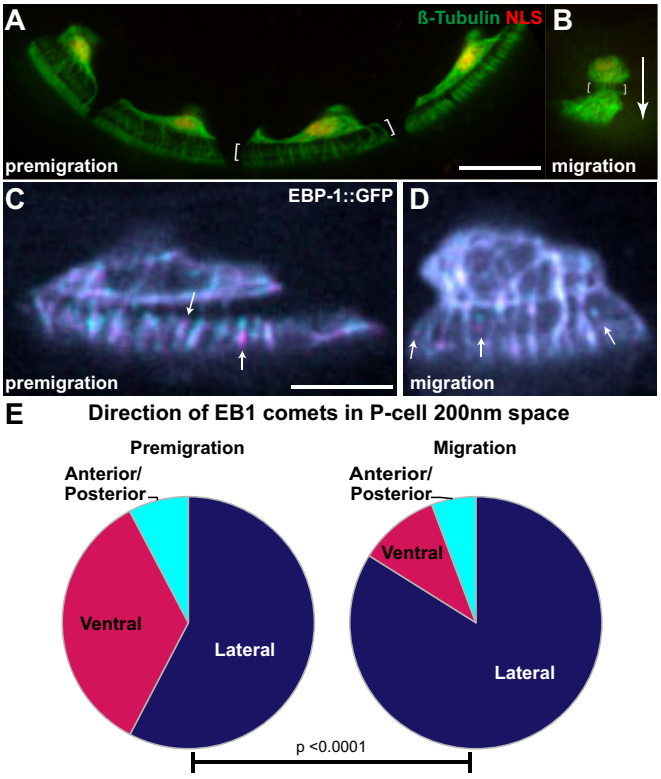

Fig. 5. Microtubules are polarized at the time of P-cell nuclear migration. (A,B) Larvae expressing β-tubulin::GFP and NLS::tdTomato in P cells. Lateral views (ventral down, anterior left) are shown and brackets mark the constrictions. Scale bar: 10 µm. (A) Four premigration cells are shown. (B) Single cell at the time of nuclear migration. Migration occurs from top to bottom, see arrow. (C,D) P cells expressing EBP-1::GFP were imaged every second for up to 3 minutes. Two frames, 5 s apart are shown with the first image pseudocolored magenta and the second cyan to show the direction of growth. Example EB1 comets in the constricted space are marked with arrows showing the direction of growth. Scale bar: 5 µm. (C) A premigration P cell at separation stage. (D) A P cell about to migrate. (E) Graphs showing the percentage of EB1 comets in the constricted space growing towards the lateral side (dark blue), the ventral side (magenta) or towards the anterior and posterior (perpendicular to axis of migration, cyan) (491 premigration comets from ten cells and 405 comets from 12 migration stage cells were analyzed). The two populations of EB1 comets are significantly different (P<0.0001 by χ^2 contingency test).

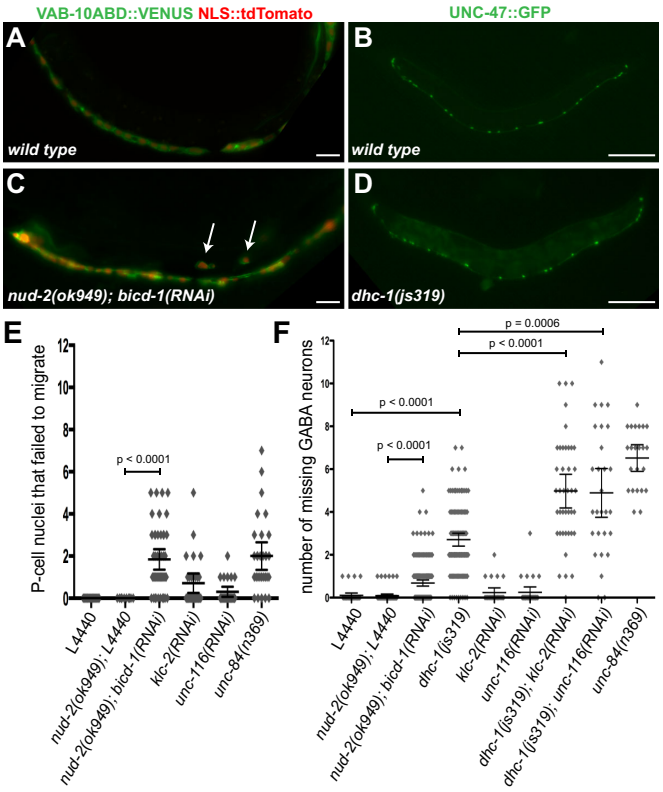

Fig. 6. Dynein and kinesin function to move P-cell nuclei. (A,C) Wild-type (A) and *nud-2(ok949);bicd-1(RNAi)* (C) late L1 larvae expressing P cell-specific (*hlh-3* promoter-driven) VAB-10ActinBindingDomain::VENUS and NLS::tdTomato. Arrows mark nuclei on the lateral side of *nud-2(ok949); bicd-1(RNAi)* larva that failed to migrate. Scale bars: 10 µm. (B,D) Wild-type (B) and *dhc-1 (js319)* (D) young adults expressing UNC-47::GFP. Lateral views, ventral down and anterior left. Scale bars: 100 µm. (E,F) Graphs of animals assayed for P-cell nuclear migration failure. Each diamond represents the number of P-cell nuclei that failed to migrate in a single animal. The bars mark mean and 95% CI. (E) Larvae assayed after the time of nuclear migration for the presence of failed P-cell nuclei on the lateral side. (F) Animals assayed as L4 larvae and young adults for the number of GABA neurons missing.

dhc-1(js319); unc-116(RNAi) animals were missing 4.9±1.09 GABA neurons (Fig. 6F). Disruption of both kinesin-1 and dynein are more severe, approaching the defects observed in *unc-84(null)* animals, which were missing 6.5±0.60 GABA neurons (Fig. 6F). Together, these data suggest dynein and kinesin-1 function together to move P-cell nuclei.

The KASH protein UNC-83 mediates dynein function during P-cell nuclear migration

In our model, microtubule motors are recruited to the surface of P-cell nuclei by the KASH protein UNC-83. We therefore hypothesized that a deletion of the dynein-binding domain of UNC-83 (Fridolfsson et al., 2010) should mimic the P-cell nuclear migration phenotype of dynein knockdowns. To test this, we used CRISPR/Cas9 to delete the cytoplasmic dynein recruitment domain in UNC-83 tagged with GFP at the endogenous locus. To engineer a functional, fluorescent-tagged UNC-83, we inserted the GFP tag on the cytoplasmic side of the UNC-83 transmembrane and KASH domains to create UNC-83::GFP::KASH. UNC-83::GFP::KASH localized at the nuclear envelope (Fig. 7A) in a pattern similar to anti-UNC-83 antibody localization (Starr et al., 2001). Furthermore, hyp7 and P-cell nuclear migration occurred normally in UNC-83::GFP::KASH transgenic animals (Fig. S2; Fig. 7). Thus, we concluded that UNC-83::GFP::KASH is functional.

We previously showed that residues 137-342 of the UNC-83c isoform interact with the kinesin light chain KLC-2 and residues 362-692 interact with dynein regulators NUD-2 and DLC-1 (Fridolfsson et al., 2010; Meyerzon et al., 2009). To test our hypothesis that the dynein-interacting domain of UNC-83 is required for normal P-cell nuclear migration, we made UNC-83(Δ344-692)::GFP::KASH transgenic animals. UNC-83(Δ344-692)::GFP::KASH localized similarly to the UNC-83::GFP::KASH construct (Fig. 7B). In UNC-83(Δ344-692)::GFP::KASH L1 larvae, 1.8±0.31 (mean± 95% CI) P-cell nuclei per animal failed to migrate (Fig. 7C), significantly more than UNC-83::GFP::KASH animals, where 0.2± 0.09 P-cell nuclei per animal failed to migrate (P<0.0001 in an unpaired t-test; n≥120). Furthermore, 0.7±0.13 GABA neurons were missing per UNC-83(Δ344-692)::GFP::KASH adult, significantly more than control UNC-83::GFP::KASH animals (P<0.0001 in an unpaired t-test; n≥200; Fig. 7D). These data suggest that UNC-83 facilitates dynein function during P-cell nuclear migration.

Development (2016) 143, 4193-4202 doi:10.1242/dev.141192

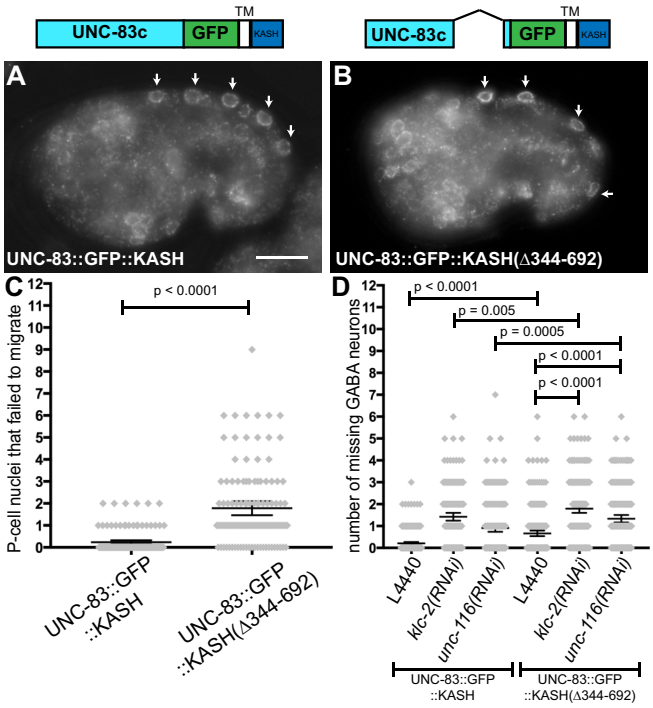

Fig. 7. UNC-83 is required to recruit dynein for P-cell nuclear migration. (A,B) Images of comma-stage embryos show normal UNC-83 localization. Arrows mark UNC-83-positive hyp7 nuclei. (A) An animal expressing UNC-83::GFP::KASH. (B) UNC-83(Δ344-692)::GFP::KASH mutant embryo. Ventral down and anterior left. Scale bar: 10 µm. (C) Graph showing larvae assayed for P-cell nuclear migration defects. (D) Graph of the number of GABA neurons missing in L4 larvae and young adult animals. Each diamond on the graphs represents a single animal; bars mark mean and 95% CI.

We then used *klc-2(RNAi)* and *unc-116(RNAi)* to knock down kinesin in UNC-83(Δ344-692)::GFP::KASH animals. Both RNAi treatments significantly enhanced the number of missing GABA neurons in UNC-83::GFP::KASH and UNC-83(Δ344-692)::GFP::KASH backgrounds (Fig. 7D), suggesting that kinesin works with dynein for P-cell nuclear migration.

DISCUSSION

Here, we established a new *in vivo* model to study nuclear migration through narrow constrictions. P-cell nuclear migration in *C. elegans* is an excellent model in which to study nuclear movements through constrictions for the following reasons. (1) Nuclear migration can be genetically separated from cell migration (Starr and Han, 2005). (2) P-cell nuclei undergo significant morphological changes (Fig. 3). (3) P-cell nuclear migration defects can be quantified by following P-cell lineages (Figs 6 and 7). (4) P-cell nuclear migration is a significant event in the life of the animal, as defects lead to loss of entire organs (Horvitz and Sulston, 1980; Sulston and Horvitz, 1981). (5) Use of P cell-specific promoters allowed us to follow components with live microscopy (Figs 3–5). (6) P-cell nuclear migration occurs in a genetically tractable system in which synthetic screens can identify new players (Chang et al., 2013; Horvitz and Sulston, 1980). (7) The molecular mechanisms for P-cell nuclear migration are likely to be conserved. For example, this system led to the discovery of SUN and KASH proteins. Thus, further studies using our P-cell nuclear migration model are expected to yield new mechanisms for nuclear migration that are likely to be conserved to mammalian systems and have implications for human health and development.

We used the P-cell model to characterize molecular mechanisms employed to move P-cell nuclei. We found that three pathways function together to mediate P-cell nuclear migration: lamins are reorganized to mediate morphological changes of nuclei, actin networks are organized to help squeeze nuclei through constrictions, and kinesin and dynein motors pull through SUN and KASH proteins to move nuclei along microtubules (Fig. 8).

Lamin expression levels were previously shown to affect nuclear migration in tissue culture. High levels of lamin inhibit nuclear deformation and squeezing through constrictions whereas low levels of lamin allow more nuclear deformation and migration (Davidson et al., 2014; Rowat et al., 2013). We examined lamin during P-cell nuclear migration using CRISPR technologies to engineer GFP::lamin expressed at endogenous levels. Our GFP::LMN-1 construct localized as expected and was partially functional (Fig. S1). Our GFP::LMN-1 transgenic protein showed that lamins were present throughout the nucleus as P-cell nuclei flattened to enter the constricted space (Fig. 3). We are working to generate a functional GFP::LMN-1 to study laminopathies (Worman, 2012) in our *in vivo* system.

The second process involved in P-cell nuclear migration is actin based. We previously used a genetic screen to identify enhancers of the nuclear migration defect of *unc-83/-84*. The first identified component is the actin nucleation regulator TOCA-1 (Chang et al., 2013). Moreover, members of the WAVE/SCAR or Arp2/3 complexes have also been implicated in P-cell nuclear migration (Xiong et al., 2011). In fact, TOCA-1 functions directly through WAVE/SCAR (Fricke et al., 2009; Giuliani et al., 2009). Together, these reports suggest that actin networks function synthetically with

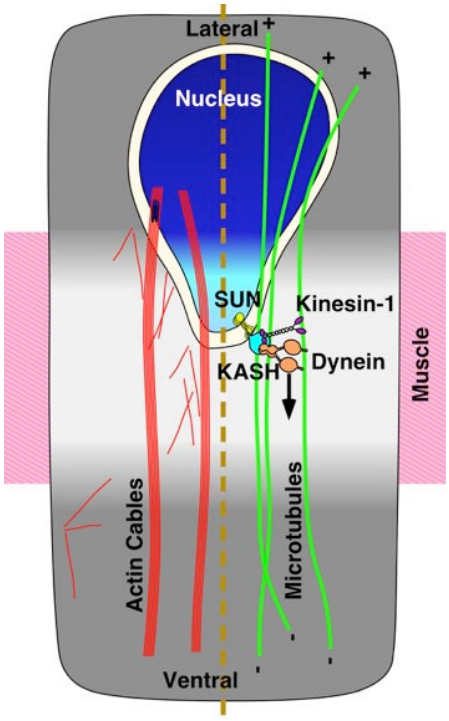

Fig. 8. Model of P-cell nuclear migration. The P-cell nucleus (blue) migrates from the lateral (top) to ventral (bottom) through a constricted space (light gray) between the muscle (pink) and the cuticle (not shown, but above the plane of the image). P-cell nuclear migration relies on a microtubule pathway consisting of polarized microtubules (green) and SUN (yellow), KASH (cyan), kinesin (purple) and dynein (tan) at the nuclear envelope. Actin cables (red) extend throughout the P cell.

Development (2016) 143, 4193-4202 doi:10.1242/dev.141192

microtubule motors recruited to the nuclear surface by SUN and KASH proteins to ensure P-cell nuclear migration. This is in contrast to nuclear migration in *C. elegans* embryonic dorsal hyp7 precursors, in which null mutations in SUN or KASH proteins disrupt nuclear migration at all temperatures (Fridolfsson and Starr, 2010; Malone et al., 1999; Starr et al., 2001). It is difficult to study the role of actin networks in hyp7 nuclear migration because defects in actin nucleators lead to defects in cellular intercalation prior to nuclear migration (Walck-Shannon et al., 2015; Xiong et al., 2011). However, given the relative severities of nuclear migration defects in hyp7 precursors versus P cells, it appears that SUN-KASH complexes and microtubule motors are essential for hyp7 nuclear migration, but are assisted by normal actin networks during P-cell nuclear migration.

We propose two models for actin participation in P-cell nuclear migration. One possibility is that myosin helps move nuclei along thick actin cables (Figs 4 and 8). Alternatively, a branched actin network at the nuclear surface could help squeeze nuclei into constrictions. This model is consistent with a role for TOCA-1 binding to the surface of the nucleus, using its F-BAR domain, only when curvature is induced. TOCA-1 could then assist the entry of the leading edge of the nucleus into the constricted space. This would place TOCA-1 in position to interact through cdc42, WAVE and/or Arp2/3 components to nucleate branched actin networks, which could provide additional shape-altering forces. In support of this model, Thiam et al. (2016) showed that actin accumulates at the opening of the constricted space as dendritic cell nuclei migrate through an *in vitro* constriction. However, we observed no gross defects in the actin network of P cells in *unc-84(n369); toca-1(tm2056)*, *toca-1(tm2056);toca-2(RNAi)* or *wve-1(RNAi)* animals, although we observed previously reported P-cell nuclear migration defects (Chang et al., 2013; Xiong et al., 2011) (data not shown). These negative results do not discount the potential involvement of branched actin networks, which are likely to be below our limit of resolution. Examination of the P-cell actin network organization in other backgrounds or precise disruption of actin-regulating components in P cells is required to resolve this question.

SUN and KASH proteins regulate the action of kinesin-1 and dynein at the nuclear surface during nuclear migration. We show that both dynein and kinesin-1 are involved in P-cell nuclear migration and disruption of both motors causes a defect similar to that observed in SUN or KASH mutants. We found that dynein disruption caused a stronger migration defect than did kinesin disruption (Fig. 6), consistent with our observation that nuclei migrated towards the minus ends of microtubules (Fig. 5). We further showed that dynein is functioning through the KASH protein UNC-83 (Fig. 7). How UNC-83 mediates the relative actions of the minus-end-directed dynein versus the plus-end-directed kinesin to move hyp7 nuclei towards plus ends of microtubules in the embryo and then to move P-cell nuclei towards minus ends in the larva requires future studies.

Most intracellular cargos are simultaneously bound to both dynein and kinesin motors and exhibit short bi-directional movements even when overall movement is directional. How opposite pulling motors are coordinated remains a major question in cell biology (reviewed by Hancock, 2014). During P-cell nuclear migration, knockdowns of both kinesin and dynein led to a more severe nuclear migration phenotype than did single knockdowns. Moreover, kinesin-1 knockdowns in UNC-83(Δ344-692)::GFP::KASH animals, which are thought to prevent dynein recruitment to the surface of the nucleus, were not as severe as dynein-kinesin double knockdowns (compare Fig. 7D with Fig. 6F). Two possibilities explain this difference. First, dynein could function at the nuclear envelope independently of UNC-83, as seen in apical nuclear migrations in neuroepithelia where dynein is recruited through nuclear pore complexes (Hu et al., 2013). Alternatively, dynein could function indirectly to mediate P-cell nuclear movement. Future studies of the coordination of dynein and kinesin motors during P-cell nuclear migration could therefore be informative for how microtubule motors move nuclei through constricted spaces, and, more generally, how cargos are moved in a bidirectional manner.

Nuclear migration through small spaces is important in hematopoiesis, inflammation and metastasis (Chow et al., 2012; Junt et al., 2007; Nourshargh et al., 2010; Shin et al., 2013; Wolf et al., 2007). However, it is usually studied in cells migrating though fabricated constrictions or collagen matrices with small openings. *C. elegans* P cells provide a new model in which to study these nuclear migrations *in vivo*. Recently, branched actin networks were shown to mediate nuclear migration in dendritic cells migrating through microchannels (Thiam et al., 2016). Findings in our P-cell model predict that TOCA-1 will be involved in regulating actin networks in dendritic cells. It will therefore be informative to translate our findings on the role of the LINC complex, microtubule motors and actin regulators, including TOCA-1, to mammalian systems to determine the extent to which these mechanisms are conserved. We also expect additional players to be identified using *C. elegans* genetics. The roles of such players can now be studied using live imaging in *C. elegans* before being translated into mammalian systems. Thus, studying P-cell nuclear migration is expected to lead to additional mechanistic insights for nuclear migration in development and metastasis.

MATERIALS AND METHODS

P cell-specific expression constructs

To express live fluorescent fusion proteins in P cells, a 3.4-kb *Hin*dIII/*Sma*I genomic fragment containing the promoter and first eight residues of *hlh-3* was cloned from pRD1 (Chang et al., 2013; Doonan et al., 2008) into pPD49.26 (gift from Andrew Fire, Stanford University School of Medicine, CA, USA; Addgene plasmid #1686) to make pSL601. To label P-cell nuclei, tdTomato with an SV40 nuclear localization signal (*nls::tdTomato*) (Spear and Erickson, 2012) was inserted downstream of the *hlh-3* promoter from pRD1 in pPD95.70 (gift from Andrew Fire; Addgene plasmid #1492) to make pSL619 (p_{hlh-3}*::nls::tdTomato*). To label tubulin and EB1 in P cells, promoters in pSL268 and pSL501 (Fridolfsson and Starr, 2010) were replaced with the *hlh-3* promoter from pSL601 to make pSL603 (p_{hlh-3}*::β-tub::gfp*) and pSL631(p_{hlh-3}*::ebp-1::gfp*), respectively. To label actin in P-cells, p_{hlh-3} was inserted before the actin-binding domain of VAB-10 (from p_{mig-24}*::vab-10abd::venus*; Kim et al., 2011) to make pSL630 (p_{hlh-3}*::vab-10abd::venus*). Lifeact, a 17-residue peptide that binds F-actin (Riedl et al., 2008) was fused to mKate2 [*C. elegans* optimized (Chen et al., 2014), from Anne-Cecile Reymann, BIOTEC TU Dresden, Germany] to create pSL780 (p_{hlh-3}*::lifeact::mKate2*).

C. elegans strains and RNAi

N2 was used as wild type (Brenner, 1974). See Table S1 for strains. Some strains were provided by the *Caenorhabditis* Genetics Center, funded by the National Institutes of Health Office of Research Infrastructure Programs (P40 OD010440). Standard microinjection techniques were used (Mello et al., 1991). Plasmids encoding P cell-specific markers were injected at 2-5 ng/µl. Transgenic strains with extra-chromosomal arrays were followed by expression of *odr-1::gfp* or *odr-1::rfp* (L'Etoile and Bargmann, 2000), which were injected at 100 ng/µl. *ycIs11* was integrated using UV/TMP treatment (Kage-Nakadai et al., 2012). RNAi knockdown experiments were performed by feeding L4 animals bacteria expressing dsRNA from the Ahringer library (Source Bioscience) (Kamath et al., 2003) at 25°C. Only progeny laid within 48 h were analyzed.

Development (2016) 143, 4193-4202 doi:10.1242/dev.141192

CRISPR/Cas9 genome editing was used to engineer UNC-83::GFP::KASH fusion proteins (Dickinson et al., 2013). Cas9 targeting sequences were cloned into pDD162 (from Bob Goldstein, University of North Carolina, Chapel Hill, NC, USA; Addgene plasmid # 47549), using Q5 site-directed mutagenesis (New England Biolabs). For the repair template, a 3.5 kb region around the 3′ end of *unc-83*, was cloned into pCR Blunt II (ThermoFisher) to make pSL714. A codon-optimized GFP (from Bob Goldstein) with six-residue (SGASGA) linkers was inserted upstream of the transmembrane domain of UNC-83 and loxP-flanked *unc-119* immediately downstream of the 3′ UTR creating pSL718. The Cas9/sgRNA construct, repair template, and injection markers were injected into *unc-119(ed3)III* animals. Integrations were identified by selecting dauers lacking injection markers. The *unc-119* cassette was removed by injecting animals with pDD104 ($P_{eft\text{-}3}$::Cre; from Bob Goldstein; Addgene plasmid # 47551) to make *unc-83(yc26[unc-83::gfp::KASH+LoxP]) V.* DNA encoding residues 344-692 of UNC-83c was deleted to make repair construct pSL748, which was injected to create *unc-83 (yc33[unc-83cΔ344-692::gfp::KASH+LoxP]).* The LoxP scar was contained in a synthetic intron.

CRISPR/Cas9 genome editing was used to tag LMN-1 with GFP at both its N and C termini. The N terminus was tagged using a GFP PCR product with 80-bp homology arms (Paix et al., 2015) co-injected with an *lmn-1* targeted sgRNA, a sgRNA to *dpy-10* and a *dpy-10(gof)* donor ssDNA (Arribere et al., 2014). Integrants were identified by finding GFP-positive animals on plates containing rollers and backcrossed three times. The C terminus was tagged using the method from Dickinson et al. (2013) and described above.

Microscopy, nuclear migration assays and image analysis

GABAergic neurons marked with *oxIs12[unc-47::gfp]* (McIntire et al., 1997) were counted as described (Chang et al., 2013; Starr et al., 2001). A complete loss of P cells would result in seven UNC-47::GFP neurons. Transgenic animals expressing *ycIs11[$p_{hlh\text{-}3}$::vab-10abd::venus; $p_{hlh\text{-}3}$::nls::tdtomato]* were used to quantify nuclear migration defects as described (Chang et al., 2013). Larva were stained with monoclonal antibody MH27 (1:200; Developmental Studies Hybridoma Bank), which recognizes AJM-1 (Francis and Waterston, 1991; Podbilewicz and White, 1994). Alexa Fluor 488-conjugated goat anti-mouse IgG secondary (1:500; A-11001, Life Technologies). P-cell nuclear migrations were assayed using a wide-field epifluorescent Leica DM6000 microscope, a 63× Plan Apo 1.40 NA objective, a Leica DC350 FX camera, and Leica LAS AF software. Fluorescent images of cytoskeletal components were captured using a spinning disc confocal microscope (Intelligent Imaging Innovations) with a CSU-X1 scan head (Yokogawa), a Cascade QuantEM 512SC camera (Photometrics) and a 100× NA 1.46 objective (Zeiss). Images were acquired using SlideBook (Intelligent Imaging Innovations). Images were processed to adjust contrast uniformly using ImageJ (National Institutes of Health).

Acknowledgements

We thank members of the Starr lab and UCD colleagues for helpful discussions, and Michael Paddy for microscopy assistance.

Competing interests

The authors declare no competing or financial interests.

Author contributions

All authors participated in experimental design. C.R.B. and S.P.M. collected and analyzed data. C.R.B., Y.-T.C. and N.E.C. created transgenic animals. C.R.B. and D.A.S. wrote the manuscript.

Funding

This work was funded by the National Institutes of Health [T32 GM007377 to C.R.B., F32 GM106730 to S.P.M., R01 GM073874 to D.A.S.]. N.E.C. is an American Cancer Society postdoctoral fellow [Illinois Division PF-13-094-01-CGC]. Deposited in PMC for release after 12 months.

Supplementary information

Supplementary information available online at
http://dev.biologists.org/lookup/doi/10.1242/dev.141192.supplemental

References

Altun, Z. F. and Hall, D. H. (2009a). Epithelial system, hypodermis. *WormAtlas*, doi:10.3908/wormatlas.1.13.

Altun, Z. F. and Hall, D. H. (2009b). Muscle system, somatic muscle. *WormAtlas*, doi:10.3908/wormatlas.1.7.

Arribere, J. A., Bell, R. T., Fu, B. X. H., Artiles, K. L., Hartman, P. S. and Fire, A. Z. (2014). Efficient marker-free recovery of custom genetic modifications with CRISPR/Cas9 in Caenorhabditis elegans. *Genetics* **198**, 837-846.

Bolhy, S., Bouhlel, I., Dultz, E., Nayak, T., Zuccolo, M., Gatti, X., Vallee, R., Ellenberg, J. and Doye, V. (2011). A Nup133-dependent NPC-anchored network tethers centrosomes to the nuclear envelope in prophase. *J. Cell Biol.* **192**, 855-871.

Bone, C. R., Tapley, E. C., Gorjanacz, M. and Starr, D. A. (2014). The C. elegans SUN protein UNC-84 interacts with lamin to transfer forces from the cytoplasm to the nucleoskeleton during nuclear migration. *Mol. Biol. Cell* **25**, 2853-2865.

Bosher, J. M., Hahn, B.-S., Legouis, R., Sookhareea, S., Weimer, R. M., Gansmuller, A., Chisholm, A. D., Rose, A. M., Bessereau, J.-L. and Labouesse, M. (2003). The Caenorhabditis elegans vab-10 spectraplakin isoforms protect the epidermis against internal and external forces. *J. Cell Biol.* **161**, 757-768.

Brenner, S. (1974). The genetics of *Caenorhabditis elegans*. *Genetics*. **77**, 71-94.

Chang, Y.-T., Dranow, D., Kuhn, J., Meyerzon, M., Ngo, M., Ratner, D., Warltier, K. and Starr, D. A. (2013). toca-1 is in a novel pathway that functions in parallel with a SUN-KASH nuclear envelope bridge to move nuclei in Caenorhabditis elegans. *Genetics* **193**, 187-200.

Chen, B.-C., Legant, W. R., Wang, K., Shao, L., Milkie, D. E., Davidson, M. W., Janetopoulos, C., Wu, X. S., Hammer, J. A., III, Liu, Z. et al. (2014). Lattice light-sheet microscopy: imaging molecules to embryos at high spatiotemporal resolution. *Science* **346**, 1257998.

Chow, K. H., Factor, R. E. and Ullman, K. S. (2012). The nuclear envelope environment and its cancer connections. *Nat. Rev. Cancer* **12**, 196-209.

Cox, E. A. and Hardin, J. (2004). Sticky worms: adhesion complexes in C. elegans. *J. Cell Sci.* **117**, 1885-1897.

Davidson, P. M., Denais, C., Bakshi, M. C. and Lammerding, J. (2014). Nuclear deformability constitutes a rate-limiting step during cell migration in 3-D environments. *Cell. Mol. Bioeng.* **7**, 293-306.

Denais, C. M., Gilbert, R. M., Isermann, P., McGregor, A. L., te Lindert, M., Weigelin, B., Davidson, P. M., Friedl, P., Wolf, K. and Lammerding, J. (2016). Nuclear envelope rupture and repair during cancer cell migration. *Science* **352**, 353-358.

Dickinson, D. J., Ward, J. D., Reiner, D. J. and Goldstein, B. (2013). Engineering the Caenorhabditis elegans genome using Cas9-triggered homologous recombination. *Nat. Methods* **10**, 1028-1034.

Doonan, R., Hatzold, J., Raut, S., Conradt, B. and Alfonso, A. (2008). HLH-3 is a C. elegans Achaete/Scute protein required for differentiation of the hermaphrodite-specific motor neurons. *Mech. Dev.* **125**, 883-893.

Feldman, J. L. and Priess, J. R. (2012). A role for the centrosome and PAR-3 in the hand-off of MTOC function during epithelial polarization. *Curr. Biol.* **22**, 575-582.

Francis, R. and Waterston, R. H. (1991). Muscle cell attachment in Caenorhabditis elegans. *J. Cell Biol.* **114**, 465-479.

Fricke, R., Gohl, C., Dharmalingam, E., Grevelhorster, A., Zahedi, B., Harden, N., Kessels, M., Qualmann, B. and Bogdan, S. (2009). Drosophila Cip4/Toca-1 integrates membrane trafficking and actin dynamics through WASP and SCAR/WAVE. *Curr. Biol.* **19**, 1429-1437.

Fridolfsson, H. N. and Starr, D. A. (2010). Kinesin-1 and dynein at the nuclear envelope mediate the bidirectional migrations of nuclei. *J. Cell Biol.* **191**, 115-128.

Fridolfsson, H. N., Ly, N., Meyerzon, M. and Starr, D. A. (2010). UNC-83 coordinates kinesin-1 and dynein activities at the nuclear envelope during nuclear migration. *Dev. Biol.* **338**, 237-250.

Fu, Y., Chin, L. K., Bourouina, T., Liu, A. Q. and VanDongen, A. M. J. (2012). Nuclear deformation during breast cancer cell transmigration. *Lab. Chip* **12**, 3774-3778.

Giuliani, C., Troglio, F., Bai, Z., Patel, F. B., Zucconi, A., Malabarba, M. G., Disanza, A., Stradal, T. B., Cassata, G., Confalonieri, S. et al. (2009). Requirements for F-BAR proteins TOCA-1 and TOCA-2 in actin dynamics and membrane trafficking during Caenorhabditis elegans oocyte growth and embryonic epidermal morphogenesis. *PLoS Genet.* **5**, e1000675.

Hancock, W. O. (2014). Bidirectional cargo transport: moving beyond tug of war. *Nat. Rev. Mol. Cell Biol.* **15**, 615-628.

Horvitz, H. R. and Sulston, J. E. (1980). Isolation and genetic characterization of cell-lineage mutants of the nematode Caenorhabditis elegans. *Genetics* **96**, 435-454.

Hresko, M. C., Williams, B. D. and Waterston, R. H. (1994). Assembly of body wall muscle and muscle cell attachment structures in Caenorhabditis elegans. *J. Cell Biol.* **124**, 491-506.

Hu, D. J.-K., Baffet, A. D., Nayak, T., Akhmanova, A., Doye, V. and Vallee, R. B. (2013). Dynein recruitment to nuclear pores activates apical nuclear migration and mitotic entry in brain progenitor cells. *Cell* **154**, 1300-1313.

Junt, T., Schulze, H., Chen, Z., Massberg, S., Goerge, T., Krueger, A., Wagner, D. D., Graf, T., Italiano, J. E., Jr, Shivdasani, R. A. et al. (2007). Dynamic visualization of thrombopoiesis within bone marrow. *Science* **317**, 1767-1770.
Kage-Nakadai, E., Kobuna, H., Funatsu, O., Otori, M., Gengyo-Ando, K., Yoshina, S., Hori, S. and Mitani, S. (2012). Single/low-copy integration of transgenes in Caenorhabditis elegans using an ultraviolet trimethylpsoralen method. *BMC Biotechnol.* **12**, 1.
Kamath, R. S., Fraser, A. G., Dong, Y., Poulin, G., Durbin, R., Gotta, M., Kanapin, A., Le Bot, N., Moreno, S., Sohrmann, M. et al. (2003). Systematic functional analysis of the Caenorhabditis elegans genome using RNAi. *Nature* **421**, 231-237.
Kim, H.-S., Murakami, R., Quintin, S., Mori, M., Ohkura, K., Tamai, K. K., Labouesse, M., Sakamoto, H. and Nishiwaki, K. (2011). VAB-10 spectraplakin acts in cell and nuclear migration in Caenorhabditis elegans. *Development* **138**, 4013-4023.
Koppen, M., Simske, J. S., Sims, P. A., Firestein, B. L., Hall, D. H., Radice, A. D., Rongo, C. and Hardin, J. D. (2001). Cooperative regulation of AJM-1 controls junctional integrity in Caenorhabditis elegans epithelia. *Nat. Cell Biol.* **3**, 983-991.
Lee, K. K., Starr, D., Cohen, M., Liu, J., Han, M., Wilson, K. L. and Gruenbaum, Y. (2002). Lamin-dependent localization of UNC-84, a protein required for nuclear migration in Caenorhabditis elegans. *Mol. Biol. Cell* **13**, 892-901.
L'Etoile, N. D. and Bargmann, C. I. (2000). Olfaction and odor discrimination are mediated by the C. elegans guanylyl cyclase ODR-1. *Neuron* **25**, 575-586.
Liu, J., Ben-Shahar, T. R., Riemer, D., Treinin, M., Spann, P., Weber, K., Fire, A. and Gruenbaum, Y. (2000). Essential roles for Caenorhabditis elegans lamin gene in nuclear organization, cell cycle progression, and spatial organization of nuclear pore complexes. *Mol. Biol. Cell* **11**, 3937-3947.
Malone, C. J., Fixsen, W. D., Horvitz, H. R. and Han, M. (1999). UNC-84 localizes to the nuclear envelope and is required for nuclear migration and anchoring during C. elegans development. *Development* **126**, 3171-3181.
McGee, M. D., Rillo, R., Anderson, A. S. and Starr, D. A. (2006). UNC-83 IS a KASH protein required for nuclear migration and is recruited to the outer nuclear membrane by a physical interaction with the SUN protein UNC-84. *Mol. Biol. Cell* **17**, 1790-1801.
McIntire, S. L., Reimer, R. J., Schuske, K., Edwards, R. H. and Jorgensen, E. M. (1997). Identification and characterization of the vesicular GABA transporter. *Nature* **389**, 870-876.
Mello, C. C., Kramer, J. M., Stinchcomb, D. and Ambros, V. (1991). Efficient gene transfer in C.elegans: extrachromosomal maintenance and integration of transforming sequences. *EMBO J.* **10**, 3959-3970.
Meyerzon, M., Fridolfsson, H. N., Ly, N., McNally, F. J. and Starr, D. A. (2009). UNC-83 is a nuclear-specific cargo adaptor for kinesin-1-mediated nuclear migration. *Development* **136**, 2725-2733.
Nourshargh, S., Hordijk, P. L. and Sixt, M. (2010). Breaching multiple barriers: leukocyte motility through venular walls and the interstitium. *Nat. Rev. Mol. Cell Biol.* **11**, 366-378.
Paix, A., Folkmann, A., Rasoloson, D. and Seydoux, G. (2015). High efficiency, homology-directed genome editing in Caenorhabditis elegans using CRISPR-Cas9 ribonucleoprotein complexes. *Genetics* **201**, 47-54.
Podbilewicz, B. and White, J. G. (1994). Cell fusions in the developing epithelia of C. elegans. *Dev. Biol.* **161**, 408-424.
Raab, M., Gentili, M., de Belly, H., Thiam, H.-R., Vargas, P., Jimenez, A. J., Lautenschlaeger, F., Voituriez, R., Lennon-Dumenil, A.-M., Manel, N. et al. (2016). ESCRT III repairs nuclear envelope ruptures during cell migration to limit DNA damage and cell death. *Science* **352**, 359-362.
Riedl, J., Crevenna, A. H., Kessenbrock, K., Yu, J. H., Neukirchen, D., Bista, M., Bradke, F., Jenne, D., Holak, T. A., Werb, Z. et al. (2008). Lifeact: a versatile marker to visualize F-actin. *Nat. Methods* **5**, 605-607.
Rowat, A. C., Jaalouk, D. E., Zwerger, M., Ung, W. L., Eydelnant, I. A., Olins, D. E., Olins, A. L., Herrmann, H., Weitz, D. A. and Lammerding, J. (2013). Nuclear envelope composition determines the ability of neutrophil-type cells to passage through micron-scale constrictions. *J. Biol. Chem.* **288**, 8610-8618.
Sakamoto, R., Byrd, D. T., Brown, H. M., Hisamoto, N., Matsumoto, K. and Jin, Y. (2005). The Caenorhabditis elegans UNC-14 RUN domain protein binds to the kinesin-1 and UNC-16 complex and regulates synaptic vesicle localization. *Mol. Biol. Cell* **16**, 483-496.
Shin, J.-W., Spinler, K. R., Swift, J., Chasis, J. A., Mohandas, N. and Discher, D. E. (2013). Lamins regulate cell trafficking and lineage maturation of adult human hematopoietic cells. *Proc. Natl. Acad. Sci. USA* **110**, 18892-18897.
Spear, P. C. and Erickson, C. A. (2012). Apical movement during interkinetic nuclear migration is a two-step process. *Dev. Biol.* **370**, 33-41.
Splinter, D., Tanenbaum, M. E., Lindqvist, A., Jaarsma, D., Flotho, A., Yu, K. L., Grigoriev, I., Engelsma, D., Haasdijk, E. D., Keijzer, N. et al. (2010). Bicaudal D2, dynein, and kinesin-1 associate with nuclear pore complexes and regulate centrosome and nuclear positioning during mitotic entry. *PLoS Biol.* **8**, e1000350.
Starr, D. A. and Fridolfsson, H. N. (2010). Interactions between nuclei and the cytoskeleton are mediated by SUN-KASH nuclear-envelope bridges. *Annu. Rev. Cell Dev. Biol.* **26**, 421-444.
Starr, D. A. and Han, M. (2005). A genetic approach to study the role of nuclear envelope components in nuclear positioning. *Novartis Found. Symp.* **264**, 208-219; discussion 219-230.
Starr, D. A., Hermann, G. J., Malone, C. J., Fixsen, W., Priess, J. R., Horvitz, H. R. and Han, M. (2001). unc-83 encodes a novel component of the nuclear envelope and is essential for proper nuclear migration. *Development* **128**, 5039-5050.
Sulston, J. E. and Horvitz, H. R. (1977). Post-embryonic cell lineages of the nematode, Caenorhabditis elegans. *Dev. Biol.* **56**, 110-156.
Sulston, J. E. and Horvitz, H. R. (1981). Abnormal cell lineages in mutants of the nematode Caenorhabditis elegans. *Dev. Biol.* **82**, 41-55.
Swift, J., Ivanovska, I. L., Buxboim, A., Harada, T., Dingal, P. C. D. P., Pinter, J., Pajerowski, J. D., Spinler, K. R., Shin, J.-W., Tewari, M. et al. (2013). Nuclear lamin-A scales with tissue stiffness and enhances matrix-directed differentiation. *Science* **341**, 1240104.
Thiam, H.-R., Vargas, P., Carpi, N., Crespo, C. L., Raab, M., Terriac, E., King, M. C., Jacobelli, J., Alberts, A. S., Stradal, T. et al. (2016). Perinuclear Arp2/3-driven actin polymerization enables nuclear deformation to facilitate cell migration through complex environments. *Nat. Commun.* **7**, 10997.
Walck-Shannon, E., Reiner, D. and Hardin, J. (2015). Polarized Rac-dependent protrusions drive epithelial intercalation in the embryonic epidermis of C. elegans. *Development* **142**, 3549-3560.
Wolf, K., Wu, Y. I., Liu, Y., Geiger, J., Tam, E., Overall, C., Stack, M. S. and Friedl, P. (2007). Multi-step pericellular proteolysis controls the transition from individual to collective cancer cell invasion. *Nat. Cell Biol.* **9**, 893-904.
Wolf, K., Te Lindert, M., Krause, M., Alexander, S., Te Riet, J., Willis, A. L., Hoffman, R. M., Figdor, C. G., Weiss, S. J. and Friedl, P. (2013). Physical limits of cell migration: control by ECM space and nuclear deformation and tuning by proteolysis and traction force. *J. Cell Biol.* **201**, 1069-1084.
Woo, W.-M., Goncharov, A., Jin, Y. and Chisholm, A. D. (2004). Intermediate filaments are required for C. elegans epidermal elongation. *Dev. Biol.* **267**, 216-229.
Worman, H. J. (2012). Nuclear lamins and laminopathies. *J. Pathol.* **226**, 316-325.
Xiong, H., Mohler, W. A. and Soto, M. C. (2011). The branched actin nucleator Arp2/3 promotes nuclear migrations and cell polarity in the C. elegans zygote. *Dev. Biol.* **357**, 356-369.
Zhao, T., Graham, O. S., Raposo, A. and St Johnston, D. (2012). Growing microtubules push the oocyte nucleus to polarize the Drosophila dorsal-ventral axis. *Science* **336**, 999-1003.